THE ASTROPHYSICAL JOURNAL, 271:865–875, 1983 August 15

ESCAPE AND IONIZATION OF ATOMIC OXYGEN FROM IO

WILLIAM H. SMYTH
Atmospheric and Environmental Research, Inc.
AND
DONALD E. SHEMANSKY
University of Southern California
Received 1982 August 11; accepted 1983 February 1

ABSTRACT

The escape of atomic oxygen from Io and its distribution in the magnetosphere of Jupiter are described in a model calculation. The loss process controlling the neutral population in this calculation is ionization by plasma electrons. The O I distribution is placed on an absolute scale by fixing the modeled 6300 Å emission intensity to the observed value. Predicted intensities for the O I 1304 Å and 880 Å emissions are included in the calculation. The model indicates a satellite emission flux of 1.5×10^{9} cm^{-2} s^{-1}, an ion loading rate of 6.2×10^{26} ions s^{-1}, an oxygen ion mass loading rate of 16.6 kg s^{-1}, and an oxygen ion energy input rate of 2.7×10^{10} W. The effect of including a neutral sulfur cloud and charge exchange reactions in the plasma torus is significant. A rough estimate including these effects raises the source flux for oxygen atoms to 1.2×10^{10} cm^{-2} s^{-1}. The inclusion of an assumed satellite flux for sulfur atoms of 6.0×10^{9} cm^{-2} s^{-1} then produces an ion loading rate of $\sim 4.0\times10^{27}$ ions s^{-1}, an ion diffusive loss time of $\sim$ 200 days, a plasma mass loading rate of $\sim$ 150 kg s^{-1}, a satellite mass loss rate of $\sim$ 270 kg s^{-1}, and a maximum ion energy input of $\sim 4\times10^{11}$ W. The energy lost by radiation (3×10^{12} W) from the *Voyager 2* epoch plasma torus exceeds the estimated energy input through the production of new ions by an order of magnitude.

Subject headings: planets: magnetospheres — planets: satellites

I. INTRODUCTION

Io, the innermost Galilean satellite of Jupiter, is known to be the source of a substantial plasma torus in the Jovian magnetosphere composed primarily of oxygen and sulfur ions. The satellite is also known to have neutral gas clouds extending spatially beyond its local gravitational control. To date, neutral gas clouds of sodium (Brown 1974), potassium (Trafton 1975; Münch, Trauger, and Roesler 1976; Trauger, Roesler, and Münch 1976), and atomic oxygen (Brown 1981) have been detected from ground-based facilities, and at least one other species, neutral sulfur, has now been reported as an observed emission by Durrance, Feldman, and Weaver (1982).

The role of the neutral gas clouds of Io as controlling factors for the maintenance and morphology of magnetospheric plasma has not been generally recognized. However, if mass is continuously lost from the plasma as it must be through various processes, neutral particles must ultimately serve as fodder for the maintenance of the system. If neutral clouds exist in the space of the plasma torus, they must certainly be a source of new ions. The recent discovery of the atomic oxygen cloud in the plasma torus remote from Io (Brown 1981) demonstrates the presence of a significant source of both plasma and energetic neutral atoms for the magnetosphere because of the recent realization that neutral-ion charge exchange reactions, in addition to electron collisions, are controlling factors in the Io plasma torus (Brown, Pilcher, and Strobel 1983; Johnson and Strobel 1982; Brown, Shemansky, and Johnson 1983; Brown and Shemansky 1982). The action of these processes is such that the characteristics of the Io atomic oxygen cloud and the properties of the magnetosphere are strongly coupled.

The significance of the recent detection by Brown (1981) of an atomic cloud near the orbit of Io, achieved by observing its electron-excited emission in the 6300 Å line, is that it provides us with the first direct information to link the escape of neutral gas from the satellite and the observed oxygen and sulfur ions in the plasma torus. The population of such neutral gas clouds in the Jovian circumplanetary space is governed by the source rate at Io and by the subsequent loss processes which occur for the escaping atoms along their orbital paths in the magnetosphere. The interaction of these clouds with the plasma torus forms the dominant sink,

converting the atoms to ions in collision with electrons and existing ions. The observation of excited emission from the O I atoms through their collision with the torus plasma electrons can then provide a means of estimating both the neutral cloud density and the resulting mass, ion, and energy input supplied to the magnetosphere by the cloud. These quantities, which are fundamental to understanding the connection of the plasma torus to the magnetosphere, have been the subject of heated discussion in the literature. The torus mass loading and diffusive loss rates have been estimated by a variety of methods (Sullivan and Siscoe 1981; Eviatar and Siscoe 1980; Richardson *et al.* 1980; Richardson and Siscoe 1981; Dessler 1980; Brown 1981; Shemansky 1980; Thorne 1981; Hill 1980), providing values separated by factors of 100 or more. An uncritical reader of the various arguments therefore cannot arrive at a sensible conclusion in regard to questions relating to how energy is delivered to the torus for its maintenance, and the nature of the interaction of the torus with Jupiter's atmosphere and magnetosphere.

The emphasis of this article will be to explore what can be learned about the escape processes of atomic oxygen from Io and the plasma source that the neutral gas forms in the planetary magnetosphere. Other plasma sources for the magnetosphere, such as direct ion escape from Io, escape of molecules such as SO_2 followed by dissociation and ionization, or escape of molecular ions such as SO_2^+ followed by dissociative processes, are also possible, but none of these processes have yet been positively identified. To explore the characteristics of the atomic oxygen cloud and its impact on the magnetosphere, a model for the gas cloud has been developed, and suitable calculations have been performed.

The model calculation requires establishment of a reasonably accurate temperature and density structure for the plasma, which we obtain from a combination of *Voyager* in situ and EUV data. The loss process providing the sink for neutral atoms in this calculation is electron impact ionization only, although we realize that charge exchange reactions are an important additional loss process in some regions of the torus. However, pending further detailed calculations, we make rough estimates below of the effect of ion-atom reactions on the atomic oxygen distribution and source rates, based on recent work by Brown, Shemansky, and Johnson (1983).

Qualitatively, the Brown (1981) observation of O I 6300 Å emission indicates a rather low abundance, implying low mass loading and source rates compared with most of the earlier published results. The energy injection rate based on the calculated production rate of ions is too low to compensate for the known radiative cooling rate. This result is not new in the published literature since Shemansky (1980) and Shemansky and Sandel (1982) have obtained similar results based on other considerations. However, there are conflicts with the other work indicated above, and the present results are by no means generally accepted. We present the model calculation below and cite the arguments and uncertainties in the issue.

II. ATOMIC OXYGEN CLOUD MODEL

Brown (1981), by adding six individual observed spectra, obtained an intensity of 8 ± 4 rayleighs in the 6300 Å emission lines. This difficult detection, which required 3 hr of integration time, was made possible by the high spectral resolution of his instrument which separated the Io emission line from the bright telluric oxygen airglow line of approximately 80 rayleighs. The Io-related emission in the 6300 Å lines is excited by inelastic impact of oxygen atoms and Io plasma torus electrons (Brown 1981). Other attempts to observe electron-impact–excited emissions of the oxygen cloud at wavelengths of 1304 Å and 880 Å, summarized in Table 1, have provided only upper limits. The plasma torus, in addition, provides a sink for the Io atomic oxygen cloud through electron impact ionization and ion charge exchange reactions. The effect of charge exchange processes, although important in the dense regions of the hot torus near Io's orbit (Brown, Shemansky, and Johnson 1983) and in the inner cool region where the torus electrons become too cold for impact ionization (Johnson and Strobel 1982), has not been included here, as mentioned earlier. The brightness of the oxygen atom emission in a

TABLE 1

OBSERVATIONAL DATA FOR THE IO ATOMIC OXYGEN CLOUD

Type of Observation	Investigator	Emission Wavelength (Å)	Brightness (rayleighs)
Ground based ...	Brown 1981	6300	8 ± 4
IUE satellite	Moos and Clarke 1981	1304	< 6
Voyager UVS	D. E. Shemansky	1304	< 25
		880	< 10

given volume element of the cloud is thus determined by the local electron number density and temperature, while the number of oxygen atoms in that volume element is determined by the previous ionization time history of these atoms in the planetary environment and the source injection rate.

Modeling the density, 6300 Å, 1304 Å, and 880 Å emission intensities, and instantaneous oxygen ion creation rate of the oxygen cloud is achieved by following in circumplanetary space the trajectories of many oxygen atoms ejected from Io and by determining proper weights along these trajectories to reflect their real-time volume excitation and ionization rates. The trajectories in circumplanetary space from the assumed isotropic ejection process at Io are determined by solving the circular restricted three-body equations of motion for each atom with suitably specified initial conditions. This procedure has been documented in detail by Smyth and McElroy (1977, 1978), who applied this method to modeling the Io sodium cloud. To determine the proper excitation and ionization weights along these trajectories, the volume excitation and ionization rates of atomic oxygen must be expressed as a function of the plasma parameters, and the plasma parameters must also be specified as a function of spatial coordinates.

The description of the plasma torus that is adopted for modeling purposes in this paper will be limited to the electrons. Ion-ion and ion-neutral collision processes will be included in future modeling when improved spatial density information for the ion species becomes available. We adopt an electron density-temperature spatial distribution based on *Voyager* experimental data. A single Maxwellian electron energy distribution is applied although we realize such a description is not strictly correct since it is known that the electrons are non-Maxwellian and that the microscopic state varies with radius and magnetic latitude within the torus (Scudder, Sittler, and Bridge 1981). This non-Maxwellian distribution is actually characterized by a dominant cool component (5–26 eV) and a small hot component (626–1200 eV). The relative abundance of the hot component measured at *Voyager 1* encounter increases with radius, having values of 0.02%, 1.38%, and 7.93% for radial values of 5.5, 7.8, and 8.9 Jupiter radii (R_J), respectively (Scudder, Sittler, and Bridge 1981). Further, observations of an upper limit of O III abundance in the hot torus (Brown, Shemansky, and Johnson 1983) have placed a stringent upper limit on the higher-energy electron component in the post–*Voyager 2* encounter epoch. According to the Brown, Shemansky and Johnson calculations, which include charge exchange reactions in the central region of the torus, the limitation on the population of hot electrons is relatively independent of ion diffusive loss time. Quantitatively, a relative hot-electron abundance of only 0.02% is above the limit indicated in the latter work. On this basis, the contribution of the hot component to the electron impact ionization and to the 6300 Å, 1304 Å, and 880 Å excitations of atomic oxygen is not significant compared with the cool-component contribution. Although ionization rate coefficients are much higher for the hot-electron component, the density relative to the cool component is too low to contribute significantly to the lifetime (see Table 2). Excitation of 6300 Å emission is inefficient at high temperatures (Table 2), whereas the excitation rates at 1304 Å and 880 Å are indeed higher (Table 2) but are offset by the low density of the hot component. Because of this, specification of only the low-temperature electron component of the plasma is required in the modeling work to follow.

Figure 1 shows the two radial temperature profiles that have been adopted in this paper for the cool electrons in the torus appropriate to the two encounter conditions of *Voyager 1* and *Voyager 2* with Jupiter. The ion temperature profile for the *Voyager 1* encounter condition is also indicated for comparison, as deduced from the in situ direct plasma measurements by Bagenal and Sullivan (1981) using their common temperature model. For radial displacements from Jupiter less than 4.9 R_J, the adopted electron temperatures in Figure 1 are assumed to have a constant value of 5.8×10^3 K (0.5 eV), whereas for radial displacements from 4.9 R_J to 5.3 R_J, values equal to the measured ion temperature are assumed. For radial distances from 5.3 R_J to 7.0 R_J, the electron temperatures are equal to average electron temperatures deduced from analysis of the extreme-ultraviolet emission from the torus ions obtained by the UVS instruments of the *Voyager 1* and *Voyager 2* spacecraft. In the 7.0–8.5 R_J region, temperatures are interpolated using the in situ measurements of Scudder, Sittler, and Bridge (1981) for the *Voyager 1* epoch, at 7.8 and 8.9 R_J. Scudder, Sittler, and Bridge (1981) also provide a measured temperature at 5.5 R_J which lies approximately 20% below the interpolated curve in Figure 1. Beyond 8.5 R_J the electron temperatures are assumed to have a constant value of 3×10^5 K (25.8 eV). The exact value of the temperature beyond 8.5 R_J is not important since ionization rates show little dependence in this temperature region. The *Voyager 2* epoch curve beyond 7.0 R_J is established by assuming the terminal temperature at 8.5 R_J was the same as the measured value at the *Voyager 1* encounter.

The radial profile of the electron number densities in the centrifugal equator of the Io plasma torus, appropriate to the encounter conditions of *Voyager 1* and *Voyager 2* with Jupiter, is shown in Figure 2. The two electron density profiles from the *Voyager 1* in situ plasma data (Bridge, Sullivan, and Bagenal 1980; Bagenal and Sullivan 1981; Bagenal 1981), deduced by equating them to the magnitude of the total ion charge density for the common temperature and thermal speed models, are shown between the radial distances of 4.0

TABLE 2

ELECTRON IMPACT IONIZATION RATE AND ELECTRON IMPACT EXCITATION RATES AT 6300 Å, 1304 Å, AND 880 Å FOR ATOMIC OXYGEN

Electron Temperature (eV)	Ionization Rate[a] ($cm^3 s^{-1}$)	6300 Å Excitation Rate[b] ($cm^3 s^{-1}$)	1304 Å Excitation Rate[b] ($cm^3 s^{-1}$)	880 Å Excitation Rate[b] ($cm^3 s^{-1}$)
0.5	6.80×10^{-21}	3.44×10^{-11}	1.99×10^{-17}	6.23×10^{-22}
1.0	7.86×10^{-15}	3.20×10^{-10}	3.61×10^{-13}	1.15×10^{-15}
2.0	1.02×10^{-11}	1.09×10^{-9}	5.50×10^{-11}	1.79×10^{-12}
5.0	1.10×10^{-9}	2.40×10^{-9}	1.27×10^{-9}	1.71×10^{-10}
10.0	7.18×10^{-9}	2.92×10^{-9}	3.01×10^{-9}	8.45×10^{-10}
20.0	2.21×10^{-8}	2.72×10^{-9}	6.68×10^{-9}	1.94×10^{-9}
50.0	4.93×10^{-8}	1.70×10^{-9}	9.04×10^{-9}	3.15×10^{-9}
100.0	6.63×10^{-8}	9.25×10^{-10}	9.45×10^{-9}	3.55×10^{-9}
200.0	7.54×10^{-8}	4.25×10^{-10}	9.00×10^{-9}	3.55×10^{-9}
500.0	7.59×10^{-8}	1.28×10^{-10}	7.70×10^{-9}	3.16×10^{-9}
1000.0	7.03×10^{-8}	4.84×10^{-11}	6.54×10^{-9}	2.74×10^{-9}
2000.0	6.19×10^{-8}	1.77×10^{-11}	5.40×10^{-9}	2.29×10^{-9}
5000.0	4.97×10^{-8}	4.56×10^{-12}	4.07×10^{-9}	1.75×10^{-9}

[a]Based on ionization cross section of Brook, Harrison, and Smith 1978.

[b]Based on O I + e calculations by Shemansky (unpublished); collision strength data for 6300 Å emission were obtained from calculations of Henry, Burke, and Sinfailam 1969; for 1304 Å, measurements by Stone and Zipf 1974 (see Shemansky 1980 for scaling factor) were used; and for 880 Å, theoretical estimates were used.

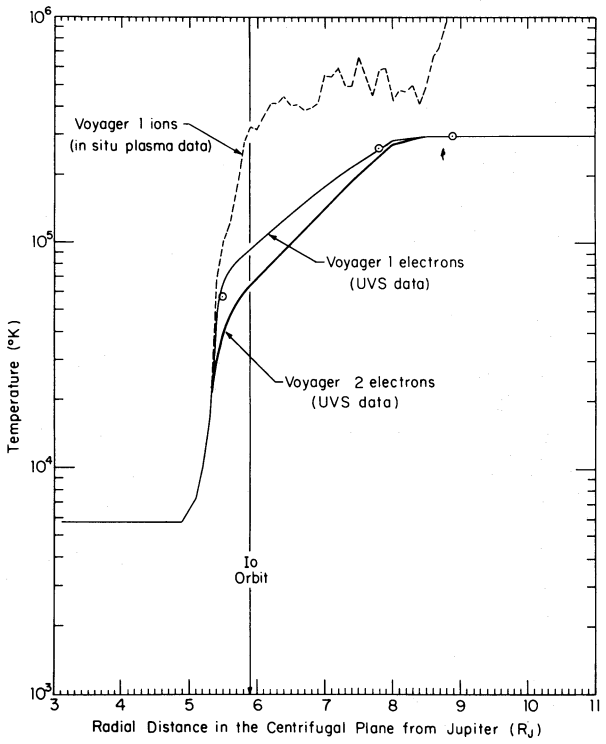

FIG. 1

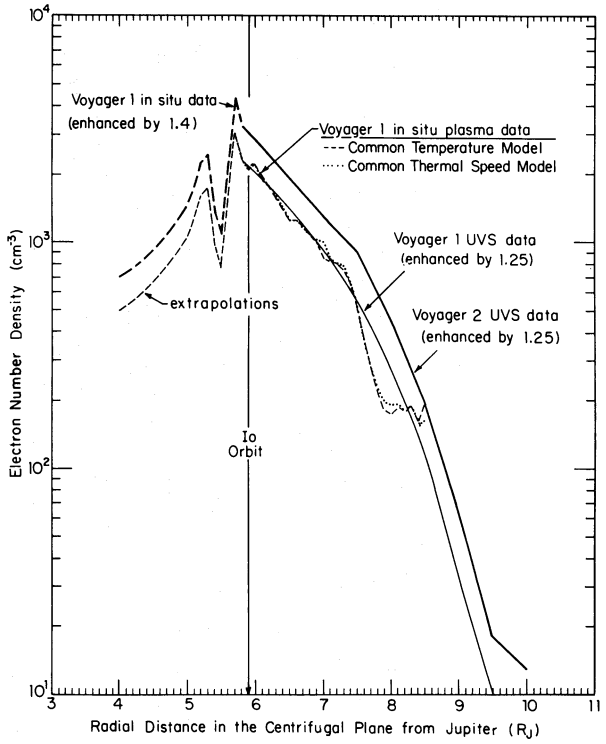

FIG. 2

FIG. 1.—Electron temperature radial profiles for the Io plasma torus. The two electron temperature profiles adopted for model calculations are discussed in the text. The plotted points are in situ measurements from Scudder, Sittler, and Bridge (1981).

FIG. 2.—Electron number density profiles for the Io plasma torus. The different number density profiles in the centrifugal plane of the plasma torus are discussed in the text. The two profiles adopted for model calculations are indicated by dashed lines for radial displacements less than 5.8 R_J and by solid lines for larger radial displacements.

R_J and 8.5 R_J. The two profiles are identical for radial displacements less than 5.8 R_J, and an extrapolated value has been assumed between 4.0 R_J and 4.9 R_J based upon refined data at 4.9 R_J and 5.0 R_J provided by Bagenal (1981). The average electron number density profiles obtained from analysis of the ultraviolet ion emission data from the plasma torus measured by the UVS instruments of *Voyager 1* and *Voyager 2* are also indicated and have been enhanced by a multiplicative factor of 1.25. This enhancement factor has been chosen to adjust the spatially averaged values of the *Voyager 1* electron density determined from the UVS data to their maximum values in the centrifugal plane as defined by the *Voyager 1* in situ plasma data. For model calculations appropriate to the *Voyager 1* encounter conditions, the adopted number densities in the centrifugal plane are defined by the in situ results from 4.0 R_J to 5.8 R_J and by the enhanced UVS results for radial displacements larger than 5.8 R_J. For model calculations appropriate to the *Voyager 2* encounter conditions, the adopted number density in the centrifugal plane will be defined by the in situ *Voyager 1* results increased by a multiplicative factor of 1.4 in the radial interval from 4.0 R_J to 5.8 R_J and by the modified UVS results of *Voyager 2* for radial displacements larger than 5.8 R_J.

In the model calculations described below, the electron number density in the Io plasma torus is specified in two dimensions, $n(r, z)$, having radial (r) and vertical (z) dependencies above and below the centrifugal plane. The number density is assumed to be independent of magnetic longitude. The two-dimensional electron number density profiles in the centrifugal plane are determined from the radial number density profiles in the centrifugal equator, $n(r)$ adopted in Figure 2, by an approximate form of a scaling law utilized earlier by Bagenal and Sullivan (1980),

$$n(r, z) = n(r) \exp\left[-(z/H)^2\right]. \quad (1)$$

In this expression the distance along the magnetic field line from the centrifugal plane has been approximated by the vertical distance from the centrifugal plane. This approximation is acceptable for the small vertical departures of interest in the Io plasma torus. The scale height H, in units of km, is defined by

$$H^2 = (1.7924 \times 10^5) \frac{T}{M}, \quad (2)$$

where the temperature T, in units of K, has been chosen as the cool-component electron temperature profile adopted in Figure 1. The value of the effective mass M, in units of amu, has been selected to be 8.2 by requiring the calculated number density $n(r, z)$ for the *Voyager 1* encounter conditions to be in reasonably good agreement with the more carefully described two-dimensional electron number density distribution reported by Bagenal and Sullivan (1981).

Having specified the spatial dependence of the electron temperature and number density in the torus, the electron-impact ionization lifetime and the 6300 Å, 1304 Å, and 880 Å volume excitation rates for atomic oxygen can be determined using the data in Table 2. The excitation rates given in Table 2 were calculated using the Brook, Harrison, and Smith (1978) measurements of the O I ionization cross section and an O I electron excitation model calculated by Shemansky (unpublished) based on available measured and theoretical collision strengths (see Table 2). The 6300 Å collision strengths, in particular, were based upon the Henry, Burke, and Sinfailam (1969) calculations. Equivalent analytic expressions were used in the model calculations. The two-dimensional electron-impact ionization lifetime for oxygen in the torus is illustrated in Figure 3 for the *Voyager 2* encounter conditions. These conditions are appropriate for the observations of Brown (1981). The motion of Io in the torus caused by the oscillation of the plasma torus about the satellite orbit plane is illustrated and causes a variation of a factor of about 6 in the oxygen lifetime at the satellite location. In the present model the centrifugal plane and the satellite orbit plane are assumed coincident so that no oscillation of the plasma is included.

To model the two-dimensional sky-plane intensity map of the 6300 Å, 1304 Å, and 880 Å emissions, many atoms are emitted from Io, and the lifetime and excitation rates along their orbits are appropriately calculated and spatially tabulated. For model results in this paper,

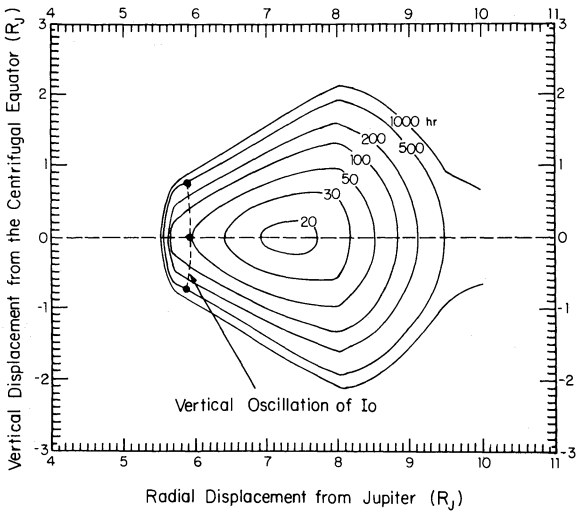

FIG. 3.—Electron-impact ionization lifetime (hr) for atomic oxygen in the Io plasma torus. The lifetime is calculated using the plasma conditions adopted for the *Voyager 2* encounter with Jupiter. Ionization cross sections are based upon the experimental measurements of Brook, Harrison, and Smith (1978).

1298 individual orbits are emitted radially and isotropically from Io's exobase (assumed 2600 km in radius), each with an initial speed of 2.6 km s^{-1}. This value of 2.6 km s^{-1} represents a likely value for the mean speed of an initial velocity dispersion and was chosen because it has been the value best suited for modeling the spatial morphology of the bright Io sodium cloud (Smyth and McElroy 1978; Smyth 1979, 1983). The implication of velocity dispersion will be discussed later. Each trajectory in the model is associated with an ensemble of oxygen atoms emitted from a surface element of the satellite exobase. In model calculations, the flight time of atom trajectories must be sufficiently long to ensure that a steady state description of the neutral gas cloud has been achieved. In all model results to follow, flight times of 500 hr and 1000 hr were suitable for the *Voyager 1* and *Voyager 2* encounter conditions, respectively. The flux of the oxygen atoms emitted from Io is determined by requiring that the calculated and measured 6300 Å intensities are identical.

III. MODEL RESULTS

The spatial morphologies of the emission intensities, neutral atom density, and ion creation rate for the Io atomic oxygen cloud have been calculated using the model described in § II. Because the only detection of the cloud has been the observation of its 6300 Å intensity (Brown 1981), model calculations to be presented will emphasize results at this wavelength and only briefly discuss intensity results for the wavelengths of 1304 Å and 880 Å.

Model results for the 6300 Å intensity on the sky plane, appropriate to the detection observation of Brown (1981), are shown in Figure 4, where *Voyager 2* plasma encounter conditions have been assumed. The two locations of Brown's observing slit are indicated, centered at 5.0 and 5.9 R_J. His intensity measurement of 8 rayleighs is an average of six 30 minute exposures, two taken at the 5.0 R_J slit location. This average intensity is achieved by our model calculation for an isotropic satellite escape flux of 1.5×10^9 atoms cm^{-2} s^{-1}, or a total source rate of 6.2×10^{26} atoms s^{-1}. The intensity contours in Figure 4, labeled in rayleighs, are evaluated for this value of the oxygen source. Using the hotter plasma conditions at the time of the encounter of *Voyager 1* with Jupiter, the neutral source rate is a factor of 2 larger, i.e., 1.2×10^{27} atoms s^{-1}.

In Figure 4, the oxygen cloud is seen to completely encircle Jupiter, having a nonuniform intensity peaked near Io and also near the elongation point of the satellite orbit. If Brown had used only one slit location and had centered it more optimally at 5.72 R_J rather than at 5.9 R_J, the model calculation predicts that a signal of 14.8 rayleighs would have been measured. The spatial variations of the 1304 Å and 880 Å intensities on the sky plane are similar in pattern to those of the 6300 Å intensity in Figure 4. The absolute intensity of the 1304 Å emission is comparable to the 6300 Å intensity for the *Voyager 1* encounter plasma conditions and about two-thirds of this value for the *Voyager 2* encounter conditions. The absolute intensity of the 880 Å emission is about a factor of 5 smaller than the 6300 Å intensity for the *Voyager 1* encounter conditions and about a factor of 10 smaller for the *Voyager 2* encounter conditions. In Table 1, the 6 rayleigh upper limit of the 1304 Å intensity determined by long-integration-time measurements of the *IUE* satellite UV instrument exceeds, because of its relatively large viewing aperture, the corresponding model-simulated value. The other upper limit for the 1304 Å emission intensity of 25 rayleighs in Table 1 was established by the *Voyager 1* UVS instrument when its much smaller rectangular viewing

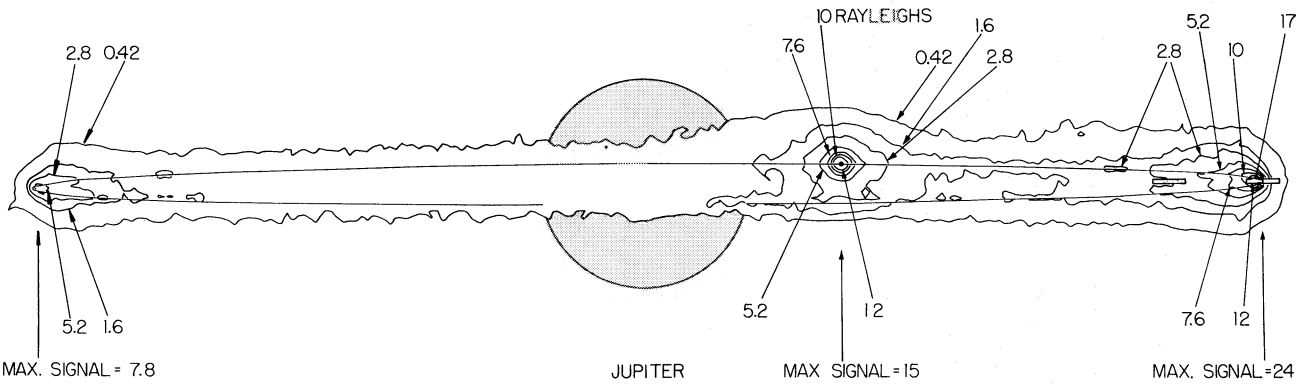

FIG. 4.—Io oxygen torus 6300 Å emission intensity. The satellite location and the calculated intensity contours are appropriate to the detection observation of Brown (1981). *Voyager 2* encounter plasma conditions and a satellitte flux of 1.5×10^9 oxygen atoms cm^{-2} s^{-1} were assumed. See text for discussion.

slit (0.5 $R_J \times 0.05$ R_J) was centered on the satellite. Near Io the model-calculated emission brightnesses are approximately symmetric north, south, east, and west of the satellite inside a radius of about 0.5 R_J. Model-calculated values of the 1304 Å intensity seen by the UV slit are 14 rayleighs for *Voyager 1* encounter conditions and 6 rayleighs for the *Voyager 2* encounter conditions, both below the measured upper limit. The 10 rayleigh upper limit of 880 Å emission intensity in Table 1 is also well above the model-calculated value.

The morphology of the 6300 Å intensity viewed from above the satellite orbit plane and corresponding to the model calculation of Figure 4 is shown in Figure 5. The intensity is brightest near Io and is moderately bright ahead of the satellite and just inside its orbit, where the temperature is still sufficiently hot to excite the line emission and where neutral oxygen is relatively abundant. The distribution of neutral oxygen is shown from the same viewing perspective in Figure 6. Oxygen atoms are seen to be concentrated primarily inside the satellite orbit, where the electrons are too cold for ionization of the cloud. Charge exchange, not included in these model calculations, will, however, modify to some extent the neutral oxygen distribution inside Io's circular orbit. The calculated instantaneous ion creation rate produced by electron impact ionization of the oxygen cloud and corresponding to the results of Figure 6 is presented in Figure 7. Ahead of Io, the ions are mostly created just inside the satellite orbit, whereas behind Io, most ions are created outside the satellite orbit and somewhat nearer the satellite where ionization lifetime has its minimum value (see Fig. 3). This overall spatial pattern is a direct consequence of the motion of neutral atoms in the gravitational force fields of Io and Jupiter and the spatial structure of the lifetime of oxygen in the plasma torus.

A radial profile for the abundance of neutral oxygen and for the ion creation rate can be produced by integrating the individual three-dimensional distributions over the angular dimension around Jupiter and the vertical dimension normal to the satellite plane. These radially averaged profiles, so constructed for radial integration-intervals of 0.1 Jupiter radii, are presented in Figure 8. The profiles were computed for the same *Voyager 2* plasma conditions and satellite emission conditions assumed in Figures 4–7. The oxygen cloud contains 2.28×10^{32} atoms, and the total ion source rate is 6.20×10^{26} ions s^{-1}. The abundance of neutral atoms is seen to decrease rapidly outside Io's orbit, while the ion creation rate is somewhat inflated because of the minimum lifetime of oxygen at 7.3 R_J (see Fig. 3). Inside Io's orbit the neutral atoms are more abundant, and the ion creation rate drops rapidly because of the precipitous decrease in the electron temperature (see Figs. 1 and 3).

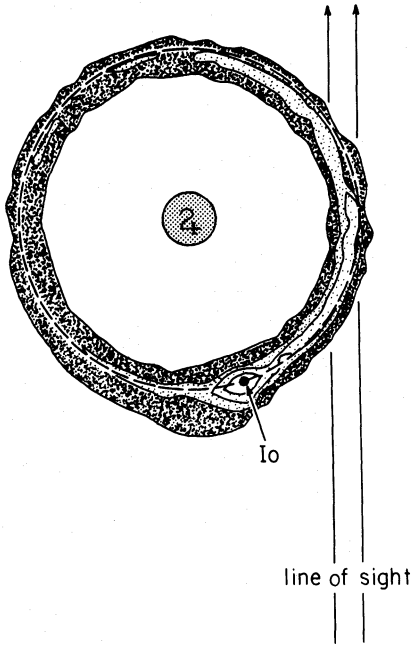

FIG. 5.—6300 Å oxygen emission intensity. The intensity morphology of the Io oxygen cloud viewed from above the satellite orbit plane is calculated for the same plasma and satellite emission conditions of Fig. 4. The intensity contours have values, in units of rayleighs, from the outer to the inner contour, of 0.045, 0.32, 0.59, and 1.13, respectively.

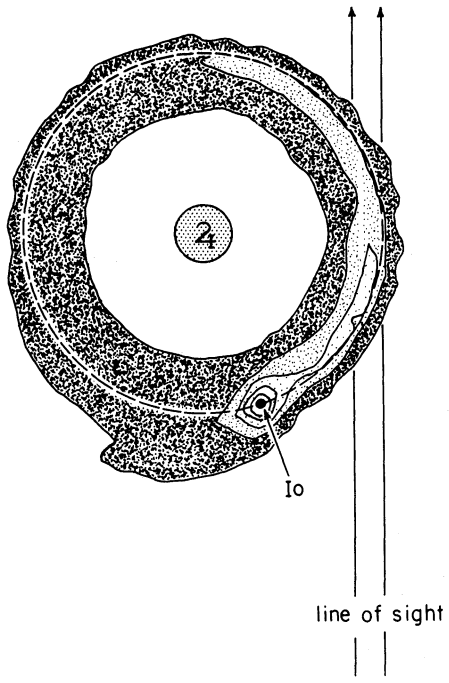

FIG. 6.—Io atomic oxygen torus. The column density morphology viewed from above the satellite orbit plane is calculated for the same plasma and satellite emission conditions of Fig. 4. The column density contours have values, in units of cm^2, from the outer to the inner contour, of 6.6×10^9, 6.7×10^{10}, 1.3×10^{11}, 1.9×10^{11}, and 3.1×10^{11}, respectively.

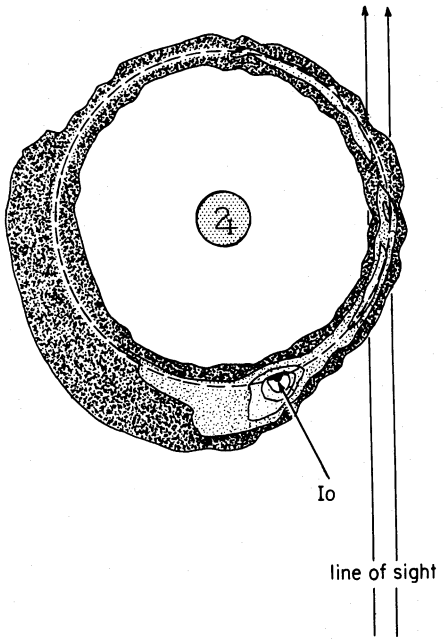

FIG. 7.—Io oxygen ion creation rate. The ion creation rate morphology viewed from above the satellite orbit plane is calculated for the same plasma and satellite emission conditions of Fig. 4. The ion creation rate contours have values, in units of ions cm^{-2} s^{-1}, from the outer to the inner contour, of 2.8×10^4, 2.0×10^5, 5.3×10^5, 8.6×10^5, and 1.4×10^6, respectively.

IV. IMPLICATIONS FOR THE PLASMA TORUS

The calculations presented in § III for the atomic oxygen cloud are a necessary first step in better understanding several physical processes that take place in the Io plasma torus. The rate at which oxygen atoms are lost by the neutral cloud may be directly used to provide a lower limit for the ion loading rate $\dot{N}$, plasma mass loading rate $\dot{M}$, and ion energy input rate $\dot{E}$ to the plasma torus. The oxygen results determine only lower limits for these three quantities since other yet unidentified direct plasma sources may also exist for the magnetosphere as well as other neutral gas clouds. The lower limit for the ion loading rate $\dot{N}$ may then be used to estimate an upper limit for the ion residence time (i.e., an ion–diffusion loss time) in the plasma torus and thereby constrain the form of the plasma diffusion coefficient for the magnetosphere.

The procedure to be utilized here for atomic oxygen may be generalized to several neutral gas clouds (O, S, etc.) where charge exchange is included and requires that only the neutral loss rates L_j and the neutral production rates P_j be calculated for each of the neutral species j. In the general case,

$$\dot{N} = -\sum_j (P_j - L_j), \tag{3}$$

$$\dot{M} = -\sum_j m_j (P_j - L_j), \tag{4}$$

$$\dot{E} = -\sum_j 1/2\, m_j \left(V_T^2 P_j - V_R^2 L_j\right), \tag{5}$$

where m_j is the mass of the jth neutral species, V_T is the average thermal velocity of an ion previous to its being converted to the jth neutral species (which then escapes the Jupiter system), and V_R is the relative velocity of an ion with respect to the rotating magnetosphere upon its being produced by ionization of the jth neutral species. The expressions for $\dot{N}$ and $\dot{M}$ follow directly from conservation requirements among the ion, electron, and neutral components, and the expression for $\dot{E}$ assumes that ion-ion charge exchange reactions do not significantly provide a net production or loss of plasma torus energy. In contrast to the plasma mass loading rate (4), a mass loss rate for the neutral cloud $\dot{M}_c$ may also be defined:

$$\dot{M}_c = \sum_j m_j L_j. \tag{6}$$

The results of § III represent the simplest case for the quantities (3)–(6), where the neutral loss rate depends only upon electron impact ionization of atomic oxygen and where the neutral production rate is zero:

$$\dot{N} = L_{\rm O}, \tag{7}$$

$$\dot{M} = \dot{M}_c = m_{\rm O} L_{\rm O}, \tag{8}$$

$$\dot{E} = 1/2\, m_{\rm O} V_R^2 L_{\rm O}. \tag{9}$$

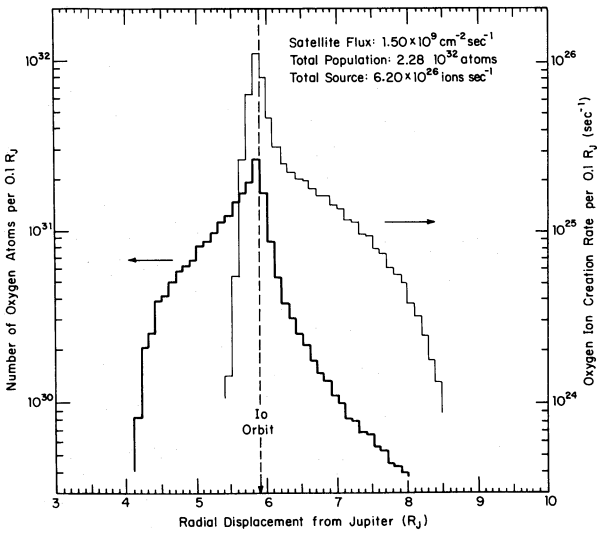

FIG. 8.—Radial profiles for oxygen abundance and ion creation rate. The profiles are calculated for the same plasma and satellite emission conditions of Fig. 4. See text for discussion.

The radial profile for L_O calculated for the plasma encounter conditions of *Voyager 2* is given in Figure 8 by the oxygen ion creation rate and produces spatially integrated source rates for $\dot{N}$, $\dot{M}$, and $\dot{E}$ of 6.2×10^{26} ions s^{-1}, 16.6 kg s^{-1}, and 2.7×10^{10} W, respectively. In calculating this last quantity, a value of 56.8 km s^{-1} for V_R was assumed and determined by the relative motion of Io and the rotating magnetosphere. An upper limit for the ion-diffusive loss time τ in the plasma torus may be estimated from $\dot{N}$ as follows:

$$\tau = \left(\frac{\dot{N}}{N}\right)^{-1}, \tag{10}$$

where N is the number of ions in the spatial element in which $\dot{N}$ is calculated. Using the spatially integrated source rate for $\dot{N}$ and an estimated total of 2.7×10^{34} ions, the averaged ion–diffusive loss time is constrained to 500 days. This relatively large value is reduced significantly when additional contributions to $\dot{N}$, roughly estimated below, are included for a sulfur gas cloud and for charge exchange processes. The spatially integrated value of 2.7×10^{10} W for $\dot{E}$, which represents less than 1% of the 3×10^{12} W radiated by the UV torus, will likewise be significantly increased by these additional contributions estimated below. For the plasma encounter conditions of *Voyager 1*, the spatially integrated source rates for $\dot{N}$, $\dot{M}$, and $\dot{E}$ are a factor of 2 larger than those given above, if it is assumed the 6300 Å intensity at this earlier time had the same brightness.

The strength of the conclusions drawn above from the results of § III are limited to some extent by several uncertainties in modeling. Inaccuracies in excitation cross sections as well as in data that specify the plasma torus properties could produce changes to increase or decrease the results. The lack of knowledge about the oxygen source characteristics of Io (i.e., the importance of higher velocity components in the dispersion of the emission velocity distribution and its exospheric distribution) could raise the overall satellite flux required to maintain the observed 6300 Å brightness, but competing processes make the overall effect difficult to estimate without further observational information about the angular extent of the atomic oxygen cloud. On the other hand, inclusion of an oscillating torus in the model would produce a longer average lifetime for atomic oxygen and would therefore likely reduce the satellite flux required to match a given 6300 Å observation. The two oppositely directed effects may to first order cancel each other.

Significant modifications of the conclusions drawn above from the results of § III may, however, be anticipated from two factors not included in the model: (1) the likely existence of a neutral sulfur cloud of Io and (2) the importance of several neutral-ion and ion-ion charge exchange reactions in the plasma torus involving the species O I, O II, O III, O IV, S I, S II, S III, and S IV. The presence of charge exchange reactions involving slow neutral atoms and fast corotating ions of the form

$$\text{neutral} + \text{ion} \rightarrow \text{ion} + \text{neutral}, \tag{11}$$

$$\text{neutral} + \text{ion} \rightarrow \text{ion} + \text{ion} \tag{12}$$

both enhances and couples the oxygen and sulfur loss rates as well as provides substantial neutral production rates. An improved model incorporating this coupling is then required to accurately describe the neutral clouds and their impact on the magnetosphere. Lacking this coupling in the present model and the necessary information about the presence of neutral sulfur in the Jovian environment, this impact may be roughly estimated by scaling the above spatially integrated model results by the model calculation of Brown, Shemansky and Johnson (1983). In their calculation, the ratio of the overall oxygen to sulfur loss rate was assumed to be 2, which is the ratio for a satellite loss rate based upon the source molecule SO_2. Using this calculation as a guide, the spatially integrated value of the oxygen loss rate L_O calculated above for electron impact ionization only is enhanced by a factor of 8 by charge exchange reactions, providing a scaled value of 5×10^{27} O I atoms s^{-1}. The spatially integrated value of the sulfur loss rate L_S is then one-half this value, or 2.5×10^{27} S I atoms s^{-1}. These two loss rates are equivalent to satellite fluxes of 1.2×10^{10} O I atoms cm^{-2} s^{-1} and 6.0×10^{9} S I atoms cm^{-2} s^{-1}, respectively. The spatially integrated values of the oxygen production rate P_O and sulfur production rate P_S may likewise be scaled using the results of Brown, Shemansky, and Johnson (1983) by factors of approximately 0.6 and 0.3 times their respective loss rates yielding values of 3.0×10^{27} O I atoms s^{-1} and 0.75×10^{27} S I atoms s^{-1}. These production rates arise from the charge exchange reactions (11) and also from electron recombination reactions.

Using these approximations for the production and loss rates for neutral oxygen and sulfur in the expressions (3) through (6), more realistic values for the ion loading rate, the plasma mass loading rate, the cloud mass loss rate, and the ion energy input rate for the plasma torus may be calculated and expressed as

$$\dot{N} = 0.75(L_O), \tag{13}$$

$$\dot{M} = 1.1(m_O L_O), \tag{14}$$

$$\dot{M}_c = 2.0(m_O L_O), \tag{15}$$

$$\dot{E} = 2.0\left(1/2 m_O V_R^2\right) L_O - 0.9\left(1/2 m_O V_T^2\right) L_O, \tag{16}$$

where the spatially integrated value of L_O is 5×10^{27} ions s^{-1}. The effects of charge exchange have thus been to modify the simple dependence exhibited among $\dot{N}$, $\dot{M}$, $\dot{M}_c$, and $\dot{E}$ in the earlier derived expressions (7), (8), and (9), which were based only on electron impact ionization. The spatially integrated value of the ion loading rate (13) is then 3.85×10^{27} ions s^{-1} and implies a value for the ion–diffusive loss time (10) of 200 days, assuming a density of 1380 cm^{-3} (appropriate to the *Voyager 2* encounter) and a plasma torus of 1 R_J radius centered on Io's orbit. The spatially integrated value of the plasma mass loading rate (14) is 146 kg s^{-1}, of which 53 kg s^{-1} are supplied by oxygen atoms and 93 kg s^{-1} by sulfur atoms. In contrast, the spatially integrated value for the mass loss rate of the neutral cloud (15) is 266 kg s^{-1}. The spatially integrated value of the ion energy input (16) is 3.9×10^{11} W, using a value of $V_T = 26.9$ km s^{-1} appropriate to the average temperature of 60 eV reported by Brown (1982) for S^+, or is 4.3×10^{11} W, using a smaller thermal speed for the ions of 7.6 km s^{-1}. These two values of the ion energy input rate represent, respectively, 13% and 14% of the 3×10^{12} W radiated by the plasma torus in UV wavelengths. This ion energy input is similar in magnitude to the Io correlated energy source discovered by Sandel and Broadfoot (1982) which supplies about 20% of the UV radiated power.

To determine the spatial variations of the ion number, mass, and energy injection rates in the plasma torus supplied by the neutral clouds, more refined model calculations (which are currently under development) will be required. The overall spatial character of these processes for oxygen or sulfur may, however, be understood as being controlled through three channels if charge exchange reactions are considered. Electron ionization in the present model would tend to dominate in radial regions more distant than 6.7 R_J. In the radial interval 5.6–6.7 R_J, roughly equal contributions from electron impact ionization and charge exchange are expected. Charge exchange reactions will dominate inside 5.6 R_J, where the electron temperature decreases rapidly. Charge exchange processes are therefore expected to modify the radial distribution of O I atoms and the ion creation rate shown in Figure 8, which are calculated only for electron impact ionization. For radial displacements larger than 5.9 R_J, the rather sharp reduction in the O I population and the substantial ion creation rate out to 7.5 R_J are caused by the rapidly rising electron ionization rate coefficient, and these features will have the same character when charge exchange is included. The drop in the ion creation rate through two decades in the inward direction from 5.9 R_J to 5.5 R_J occurs because of the precipitous drop in the electron temperature in that region. The inclusion of charge exchange reactions will provide a new ion production mechanism inward of 5.9 R_J which will enhance the ion creation rate and will also sharpen the neutral atom distribution by reducing the relative number of atoms in the 4.5–5.5 R_J region. The extent of the oxygen cloud will also be confined more closely to the position of Io, and the radial distribution of oxygen may then tend to show a slightly higher density peak than that shown in Figure 8, because the Brown (1981) observation was made ~ 90° downstream from the position of Io.

The above estimates for the ion loading rate, the mass loading rate, and the ion energy loading rate for the plasma torus have as their source the neutral gas clouds of Io. Although it is almost certain that Io is the ultimate source of these ions, other sources of neutral atoms or direct sources of ions that have yet to be discovered might also exist in addition to the ions created by the neutral gas clouds. If the other sources of ions are significant, the above estimates of $\dot{N}$, $\dot{M}$, and $\dot{E}$ are only lower limits. It is difficult to assess the possible magnitude of direct ion sources since knowledge of Io's atmosphere and the mechanisms which deliver the material to the torus is very limited. Only oxygen ionization processes that occur in the near vicinity of Io have been limited by direct observation and predictable emission efficiencies (Shemansky 1980). The Shemansky (1980) upper limit on direct ion injection from Io is roughly 10^{27} s^{-1} based on ion detection of the O I 1304 Å line in *Voyager 1* observations. Attempts to observe the 1304 Å line by Moos and Clarke (1981) using the *IUE* satellite produce about the same value, 10^{27} s^{-1}, as an upper limit for the *Voyager 1* encounter epoch. It is likely that the source molecule supplying the neutral gas clouds is SO_2 (Pearl *et al.* 1979; Johnson *et al.* 1979) so that direct escape of SO_2, SO_2^+ or its chemical fragments (SO, O_2, etc.) may occur and may not have been detected as yet. The assessment of the importance of these molecules and ions as a source of plasma for the magnetosphere will, however, depend upon the acquisition of additional information.

V. CONCLUDING REMARKS

A model has been presented for the neutral oxygen cloud of Io based upon atom-electron impact excitation and ionization processes in the plasma torus. The flux of oxygen atoms emitted from Io was determined by requiring that the measured (Brown 1981) and the calculated 6300 Å intensities be identical. By this means satellite emission fluxes of 3.0×10^9 cm^{-2} s^{-1} and 1.5×10^9 cm^{-2} s^{-1} were required for plasma conditions appropriate to the times of encounter of *Voyager 1* and *Voyager 2* with Jupiter. The 6300 Å observations of Brown (1981) were more appropriate to the *Voyager 2* plasma conditions, for which spatially integrated ion loading rates, plasma mass loading rates, and ion energy input rates were calculated to be 6.2×10^{26} ions s^{-1}, 16.6 kg s^{-1}, and 2.7×10^{10} W, respectively. This value of

the ion loading rate implies an ion-diffusive loss time of 500 days.

Enhanced values of the satellite emission flux, ion loading rate, mass loading rate, and ion energy input rate resulting from the presence of a likely existing sulfur cloud and from the impact of charge exchange reactions were then roughly estimated based on the results of the oxygen model and the charge exchange calculations of Brown, Shemansky, and Johnson (1983). The upward adjusted value of the satellite flux for atomic oxygen was 1.2×10^{10} cm^{-2} s^{-1}, and an additional satellite flux of 6.0×10^{9} cm^{-2} s^{-1} was assumed for the likely existing sulfur cloud of Io. This represents a neutral mass loss for the satellite of ~ 270 kg s^{-1}. The corresponding adjusted values for the spatially integrated ion loading rate, plasma mass loading rate, and ion energy input rate were then 3.8×10^{27} ions s^{-1}, ~ 150 kg s^{-1}, and $(3.9\text{–}4.3)\times10^{11}$ W, respectively. This value for the ion loading rate implies an ion–diffusive loss time of ~ 200 days. The value of the ion energy input rate represents about 13%–14% of the 3×10^{12} W radiated in the UV by the plasma torus and is comparable to the 20% energy input level associated with the Io correlated energy source discovered by Sandel and Broadfoot (1982). The remaining 80% of the energy input has been associated by Shemansky and Sandel (1982) with a local time asymmetry in the electron temperature.

Inclusion of charge exchange reactions in future models of the atomic oxygen cloud is important both in refining the values of physical quantities roughly estimated above and in providing an interpretative base for new observations of the neutral and ion species of the magnetosphere. Such a model is presently under development. New observations of the angular distribution of atomic oxygen around Jupiter would be particularly useful in refining the value of the oxygen flux emitted by Io. Observations to detect an atomic sulfur cloud are likewise desirable in order to establish a satellite emission flux for sulfur and thereby better understand processes in the local atmosphere of Io.

The contributions of W. H. Smyth and D. E. Shemansky were supported by the NASA Earth and Planetary Exploration Division, Planetary Atmospheres Discipline, grants NASW-3503 and NAGW-106, respectively. We wish to thank D. M. Hunten for an editorial reading of the paper. W. H. Smyth wishes to thank M. R. Combi for contributions to the program and for helpful discussion.

REFERENCES

Bagenal, F. 1981, private communication.
Bagenal, F., and Sullivan, J. D. 1980, *Geophys. Res. Letters*, **7**, 41.
_____. 1981, *J. Geophys. Res.*, **86**, 8447.
Bridge, H. S., Sullivan, J. D., and Bagenal, F. 1980, private communication.
Brook, E., Harrison, M. F. A., and Smith, A. C. H. 1978, *J. Phys. B.*, **11**, 3115.
Brown, R. A. 1974, in *IAU Symposium 65, Exploration of the Planetary System*, ed. A. Woszczyk and C. Iwaniszewska (Dordrecht: Reidel), pp. 527–531.
_____. 1981, *Ap. J.*, **244**, 1072.
_____. 1982, *J. Geophys. Res.*, **87**, 230.
Brown, R. A., Pilcher, C. B., and Strobel, D. F. 1983, in *Physics of the Jovian Magnetosphere*, ed. A. J. Dessler (New York: Cambridge University Press), p. 197.
Brown, R. A., and Shemansky, D. E. 1982, *Ap. J.*, **263**, 433.
Brown, R. A., Shemansky, D. E., and Johnson, R. E. 1983, *Ap. J.*, **264**, 309.
Dessler, A. J. 1980, *Icarus*, **44**, 291.
Durrance, S. T., Feldman, P. D., and Weaver, H. A. 1982, *EOS Trans. American Geophys. Union*, **63**, 369.
Eviatar, A., and Siscoe, G. L. 1980, *Geophys. Res. Letters*, **7**, 1085.
Henry, R. J. W., Burke, P. G., and Sinfailam, A. L. 1969, *Phys. Rev.*, **178**, 218.
Hill, T. W. 1980, *Science*, **207**, 301.
Johnson, R. E., and Strobel, D. F. 1982, *J. Geophys. Res.*, **87**, 10385.
Johnson, T. V., Cook, A. F., Sagan, C., and Soderblom, L. A. 1979, *Nature*, **280**, 246.
Moos, H. W., and Clarke, J. T. 1981, *Ap. J.*, **247**, 354.
Münch, G., Trauger, J., and Roesler, F. 1976, *Bull. AAS*, **8**, 467.
Pearl, J., *et al.* 1979, *Nature*, **280**, 755.
Richardson, J. D., and Siscoe, G. L. 1981, *J. Geophys. Res.*, **86**, 8485.
Richardson, J. D., Siscoe, G. L., Bagenal, F., and Sullivan, J. D. 1980, *Geophys. Res. Letters*, **7**, 37.
Sandel, B. R., and Broadfoot, A. L. 1982, *J. Geophys. Res.*, **87**, 212.
Scudder, J. D., Sittler, E. C., Jr., and Bridge, H. S. 1981, *J. Geophys. Res.*, **86**, 8157.
Shemansky, D. E. 1980, *Ap. J.*, **242**, 1266.
Shemansky, D. E., and Sandel, B. R. 1982, *J. Geophys. Res.*, **87**, 219.
Smyth, W. H. 1979, *Ap. J.*, **234**, 1148.
_____. 1983, *Ap. J.*, **264**, 708.
Smyth, W. H., and McElroy, M. B. 1977, *Planet. Space Sci.*, **25**, 415.
_____. 1978, *Ap. J.*, **226**, 336.
Stone, E. J., and Zipf, E. C. 1974, *J. Chem. Phys.*, **60**, 4237.
Sullivan, J. D., and Siscoe, G. L. 1981, in *Satellites of Jupiter*, ed. D. Morrison (Tucson: University of Arizona Press).
Thorne, R. M. 1981, *Geophys. Res. Letters*, **8**, 509.
Trafton, L. 1975, *Nature*, **258**, 690.
Trauger, J., Roesler, F., and Münch, G. 1976, *Bull. AAS*, **8**, 468.

DONALD E. SHEMANSKY: Space Science Institute, University of Southern California, 3625 East Ajo Way, Tucson, AZ 85713

WILLIAM H. SMYTH: Atmospheric and Environmental Research, Inc., 840 Memorial Drive, Cambridge, MA 02139